Multimodal Imaging Mass Spectrometry to Identify Markers of Pulmonary Arterial Hypertension in Human Lung Tissue using MALDI-ToF, ToF-SIMS and Hybrid SIMS

Sebastiaan van Nuffel, Marceau Quatredeniers, Alexander Pirkl, Julia Zakel, Jean-Pierre Le Caër, Nicolas Elie, Quentin Vanbellingen, Sébastien Joël Dumas, Morad Nakhleh, Maria Rosa Ghigna, et al.

Multimodal Imaging Mass Spectrometry to Identify Markers of Pulmonary Arterial Hypertension in Human Lung Tissue using MALDI-ToF, ToF-SIMS and Hybrid SIMS

Sebastiaan Van Nuffel[1†], Marceau Quatredeniers[2,3], Alexander Pirkl[4], Julia Zakel[4], Jean-Pierre Le Caer[1], Nicolas Elie[1], Quentin P. Vanbellingen[1‡], Sébastien Joël Dumas[2,3§], Morad Kamel Nakhleh[2,3], Maria-Rosa Ghigna[2,3], Elie Fadel[2,3], Marc Humbert[2,3,5], Pierre Chaurand[6], David Touboul[1], Sylvia Cohen-Kaminsky[2,3*††], Alain Brunelle[1,7*††]

1 Université Paris-Saclay, CNRS, Institut de Chimie des Substances Naturelles, UPR 2301, 91198, Gif-sur-Yvette, France.

2 Université Paris-Saclay, School of Medicine, Le Kremlin-Bicêtre, France

3 INSERM UMR_S 999 «Pulmonary Hypertension: Pathophysiology and Novel Therapies», Hôpital Marie Lannelongue, Le Plessis-Robinson, France

4 IONTOF GmbH, Heisenbergstraße 15, 48149 Münster, Germany

5 Assistance Publique - Hôpitaux de Paris (AP-HP), Department of Respiratory and Intensive Care Medicine, Pulmonary Hypertension National Referral Center, Hôpital Bicêtre, Le Kremlin-Bicêtre, France.

6 Department of Chemistry, Université de Montréal, Montréal, QC, Canada

7 Laboratoire d'Archéologie Moléculaire et Structurale, LAMS UMR8220, CNRS, Sorbonne Université, 4 place Jussieu, 75005 Paris, France

* Corresponding Authors: E-mail: alain.brunelle@cnrs.fr, sylvia.cohen-kaminsky@universite-paris-saclay.fr.

ABSTRACT: Pulmonary arterial hypertension (PAH) is a rare and deadly disease affecting roughly 15-60 people per million in Europe with a poorly understood pathology. There are currently no diagnostic tools for early detection nor does a curative treatment exist. The lipid composition of arteries in lung tissue samples from human PAH and control patients were investigated using matrix-assisted laser desorption ionization (MALDI) imaging mass spectrometry (IMS) combined with time-of-flight secondary ion mass spectrometry (TOF-SIMS) imaging. Using random forests as an IMS data analysis technique, it was possible to identify the ion at *m/z* 885.6 as a marker of PAH in human lung tissue. The *m/z* 885.6 ion intensity was shown to be significantly higher around diseased arteries and was confirmed to be a diacylglycerophosphoinositol PI(C18:0/C20:4) via MS/MS using a novel hybrid SIMS instrument. The discovery of a potential biomarker opens up new research avenues which may finally lead to a better understanding of the PAH pathology and highlights the vital role IMS can play in modern biomedical research.

Introduction

Pulmonary arterial hypertension (PAH) is a rare and fatal disease, which affects 15 to 60 people per million in Europe[1]. PAH is a subtype of the pulmonary hypertension family that is characterized by an intense remodelling of the small pre-capillary pulmonary vessels. The progressive obstruction of the pulmonary arteries leads to an increased mean pulmonary arterial pressure (> 20 mmHg) causing right heart hypertrophy and ultimately heart failure and death[2]. In addition, PAH is also characterized by increased pulmonary vascular resistance (≥ 3 WO) and decreased pulmonary artery wedge pressure (≤ 15 mmHg). PAH has a wide range of aetiologies and can be idiopathic, inherited (e.g. genetic mutations), induced by drugs or toxins (e.g. chemotherapies, professional exposure to solvents, etc.) or associated with diseases, which can be both congenital and acquired. Despite the improved understanding of the PAH pathophysiology and the great advances in the therapeutic field over the past 20 years, there is still no curative treatment and one of the patient's only treatment options remains lung transplantation. Recent reports attest that the overall survival rate is about 52-75% 5 years after diagnosis, and 45-66% after 10 years. Unfortunately, this high mortality rate is related to the late manifestation and the non-specificity of symptoms such as dyspnoea, sleep apnoea, thoracic pain and eventually syncopal episodes. Being a rare disease, PAH diagnosis is only considered after many other possible diseases were ruled out. Therefore, there is an urgent need to uncover new and early specific biomarkers that could help practitioners to diagnose PAH at its earliest stage as well as new therapeutic strategies that could thwart the development of the disease.

Over the past two decades, imaging mass spectrometry (IMS) has arisen as a powerful tool to answer research questions in the biomedical field[3,4,5]. The medical and biological disciplines have hitherto relied on microscopy techniques which require specific antibodies and fluorescence labelling. Due to spectral overlap, one is usually limited to 3-5 fluorescent labels for a

single imaging experiment[6]. Imaging mass spectrometry on the other hand allows for label-free chemical imaging. Moreover, unlike SEM-EDS and Raman microscopy which respectively only provide elemental and chemical bond information, imaging mass spectrometry provides full molecular information. In other words, IMS can map the distribution of proteins, lipids, carbohydrates, metabolites, drugs and toxins in tissues and cells without any need for antibodies and isotopic tracers. In order to detect possible biomarkers for pulmonary arterial hypertension (PAH), we used MALDI and ToF-SIMS IMS to investigate human lung tissue samples from patients with PAH and without PAH (referred to as controls) to look for differences in their lipid composition. Although ToF-SIMS is frequently used to image the lipid distribution in tissue sections[7,8,9], previous research performed on lung tissue reported the detection of nanoparticles in rat lung tissue[10,11,12,13] and, so far, only a few reports have been published where mouse lung tissue sections have been investigated biologically[14,15]. Recently a ToF-SIMS analysis of human lung tissue revealed increased iron deposition in the context of chronic obstructive pulmonary disease[16], and MALDI has been used recently on human lung tissue to detect accumulation of metabolites relevant to disease mechanisms in PAH human lung sections[17].

One of the reasons IMS is underused in the biomedical sciences is the lack of powerful data analysis tools as these hyperspectral techniques generate very large data sets. ToF-SIMS mass spectra in particular are notoriously complex and library approaches have failed so far mainly due to the poorly understood matrix effects that occur and its complex ion formation mechanism[18,19]. Furthermore, biological systems are a very complex mixture of molecules that often contain the same building blocks. For these reasons, multivariate analysis tools have been adopted to reduce the complexity of these data sets[20,21,22]. In the past, exploratory data analysis techniques such as Principal Component Analysis (PCA) have shown to be incredibly useful in segmenting image data and finding positive correlations between mass peaks[23,24]. However, in this study the goal was to classify tissue sections into PAH and control patient tissue based on the chemistry that sets them apart. Here, we demonstrate how supervised machine learning algorithms such as Random Forests perform better for classification problems such as disease biomarker discovery using IMS[25,26].

Finally, one additional challenge of using ToF-SIMS for biomarker discovery is the difficulty to assign a molecule to a certain mass peak. In a typical ToF-SIMS instrument one must rely on the mass and isotopic pattern of a molecular ion and its positive correlations with lower mass fragments to help identify its structure, which leaves ample ambiguity[27]. In 2016, the Hybrid SIMS was launched, which was developed at IONTOF in collaboration with the National Physical Laboratory (NPL) and Thermo Fisher Scientific as well as experts in drug discovery at GlaxoSmithKline and pharmaceutical science at the University of Nottingham[28]. This instrument combines a conventional ToF-SIMS instrument with a Q-Exactive Orbitrap™, which allows for tandem MS[29]. Because the fragment ions are generated through collision-induced dissociation (CID), it is also possible to use direct spectrum-to-spectrum matching against a reference library of previously observed MS/MS. The Orbitrap mass analyser also has an incredibly high mass resolution up to 240,000 at *m/z* 200 and a mass accuracy below 1 ppm. These analytical performances allow to determine the chemical formula of each fragment ion in the MS/MS spectrum often without any ambiguity. In this study, we demonstrate the powerful capabilities of this new type of instrument.

Materials and Methods

Human tissues. Lung samples were obtained from PAH patients (see Table S1) undergoing lung transplantation or from control subjects during pneumonectomy for localized lung cancers. In control lung specimens, the pulmonary arteries studied were located far away from the tumour areas. PAH was diagnosed by cardiac catheterization at the National Reference Center for PAH, in a program approved by the *Comité de Protection des Personnes Ile-de-France VII*. Every patient signed an informed consent for participation in the study (protocol N8CO-08- 003, ID RCB: 2008-A00485-50). Lung histology was assessed by a pathologist from the pathology department after transplantation or pneumonectomy, confirming both PAH and control groups.

Sample Preparation. The lung tissue was sectioned (6 µm) at -20°C using a CM3050-S cryomicrotome (Leica, Nanterre, France). For each lung sample, serial sections were numbered from 1 to 5. For each series, sections 1, 2, 4 and 5 were thaw-mounted on conductive ITO-coated glass microscope slides and directly stored at -80°C for IMS (Figure S1). Section 3 (middle of the series) was thaw-mounted on a glass microscope slide and used for histology.

Histological staining. Frozen sections were fixed with 4% paraformaldehyde for 10 minutes at room temperature. After a wash with tap water, fixed sections were stained with haematoxylin for 1 minute. After a new wash, they were counterstained with erythrosine for 3 seconds, and washed again. Sections were viewed under a Zeiss Axio Observer Z1 (Zeiss, Marly-le-Roi, France) and images were recorded and analysed with Axiovision 4.8 software (Zeiss).

Matrix Deposition and MALDI-TOF IMS. Prior to MALDI matrix application, tissue sections were dehydrated in a vacuum desiccator for at least 30 minutes. Dehydrated samples were kept in a vacuum desiccator between manipulations or for prolonged storage. About 300 $\mu g \cdot cm^{-2}$ of 1,5-diaminonaphthalene (DAN, Sigma-Aldrich, St. Louis MO, USA - 56451) was applied to the sections by sublimation using a home-built sublimation system[30]. Because we were still in the exploration phase of our study in the case of the MALDI IMS experiments, it was important to measure in both positive and negative polarity. DAN matrix is especially suited for high spatial resolution lipid imaging in both positive and negative ion modes. It was also important to obtain a good lateral resolution and the best lateral resolution is achieved using sublimation as a MALDI matrix deposition method[24]. 0.2 µL of PepMix 5 (LaserBiolabs, Nice, France) was pipetted onto the matrix next to the tissue sample for external mass calibration. All MALDI IMS experiments were performed using a MALDI-TOF/TOF (ultrafleXtreme, Bruker Daltonics, Wissembourg, France) in reflectron mode. Pixel size was set to 15 µm with 100 shots per pixel. Mass spectra were recorded in negative polarity in the *m/z* 480 - 1900 range.The raw spectra for each individual pixel were imported into Matlab for further data processing and analysis using in-house generated Matlab scripts. All calculations were performed on a 64-bit Windows 10 platform with 64 GB of RAM, using a 3.60 GHz Intel® Xeon® E3-1270 v5 processor.

Matrix Deposition and MALDI-TOF/TOF MS. A 10 $mg \cdot mL^{-1}$ 9-aminoacridine (9AA, Sigma-Aldrich, St. Louis MO,

USA - 92817) solution was prepared by dissolving 9AA in ethanol/H_2O 70 /30 V/V % ethanol solution. The MALDI MS/MS experiments were conducted at the end of the study where the main consideration was to generate a high amount of the precursor ion in the negative polarity, and 9AA matrix is especially suited for the analysis of lipids in the negative ion mode[31]. Given that imaging was not of interest, we used a well-established spray-coating protocol for matrix application. The fifth lung tissue section from 1 PAH patient (ID: PAH6) was homogeneously coated with the matrix solution using a TM-Sprayer (HTX Technologies, Carrboro, NC, USA) at 100 °C in a single coating step with a movement speed of 120 cm·min^{-1}, nebulized nitrogen pressure of 10 psi and pump flow rate of 0.24 mL·min^{-1}. The MALDI MS/MS experiment was performed using a MALDI-TOF/TOF (ultrafleXtreme, Bruker Daltonics, Wissembourg, France). Pixel size was set to 15 µm with 500 shots per pixel. Mass spectra were recorded in negative polarity in the *m/z* 40 - 1775 range. The ion peak at *m/z* 885.7 was selected as the precursor ion for the MS/MS experiment. (LaserPower = 49%; SmartBeam Size = Ultra; Laser Frequency = 1000 Hz).

ToF-SIMS Imaging. Prior to SIMS imaging, tissue sections were dehydrated in a vacuum desiccator for at least thirty minutes. Dehydrated samples were kept in a vacuum desiccator between manipulations or for prolonged storage. The ToF-SIMS analyses were performed using a TOF-SIMS IV instrument (IONTOF GmbH, Münster, Germany) equipped with a Bi liquid metal ion gun (LMIG). The primary ion beam is directed at the sample under an angle of 45° in relation to the normal and has a beam spot of 1-2 µm in the so-called high-current bunched mode. 25 keV energy Bi_3^+ primary ions were used in all measurements. Charging of the sample is compensated with the low-energetic 20 eV electrons of the flood gun. Ion images were recorded in the high-current bunched mode, which allows for higher mass resolution[32]. The images were acquired on a surface of 500 µm × 500 µm raster scans with 512 × 512 pixels (~1 µm pixel size) and 32 scans (1 shot per pixel) were analyzed. With a Bi_3^+ current of 0.32 pA in AC (cycle time of 150 µs) mode, this resulted in an ion dose of 1×10^{12} primary ions per cm^2. All spectra were internally calibrated using the same ions, namely CH^- at *m/z* 13.0084, C_2^- at *m/z* 24.0005, C_3^- at *m/z* 36.0005, C_4^- at *m/z* 48.0005, $C_{14}H_{27}O_2^-$ at *m/z* 227.2017 (C14:0 fatty acid [FA]), $C_{16}H_{31}O_2^-$ at *m/z* 255.2330 (C16:0 FA), $C_{18}H_{35}O_2^-$ at *m/z* 283.2643 (C18:0 FA) and $C_{27}H_{43}O^-$ at *m/z* 383.3319 (cholesterol). Via thresholding using the palmitate anion ($C_{16}H_{31}O_2^-$) at *m/z* 255.23 as a marker for biological tissue material, mass spectra that exclude contributions from the OCT background were reconstructed with the commercial IONTOF software (SurfaceLab 6.7). These reconstructed mass spectra were then exported in an ASCII file format and imported into Matlab for further data processing with in-house generated Matlab scripts.

Hybrid SIMS MS/MS. One area of section 5 of PAH patient (ID: PAH2) was analyzed using IONTOF's new Hybrid SIMS instrument[28]. The negative polarity MS/MS spectrum of the ion at *m/z* 885.6 was recorded using the Thermo Scientific™ Q Exactive™ HF Orbitrap using a collision energy of 56.7 eV. Primary ions used were Ar_n clusters (n ≈ 1900) at 5 keV, and a primary ion dose density roughly equal to 1.5×10^{14} primary ions per cm^2 over an area of 500 µm × 500 µm.

Statistical Analysis. After a list of relevant mass peaks emerged as potential biomarkers for PAH, their average normalised ion intensities were calculated for each tissue section and subjected to a two tailed t-test to determine if there are significant differences between consecutive lung sections.

Results

MALDI IMS. Negative polarity ion images from three consecutive lung tissue sections of one PAH patient (ID: PAH1) and three consecutive lung tissue sections of one control patient (ID: CTRL1) were collected using MALDI IMS. Images were taken around occluded arteries in the tissue sections of the PAH patient and around normal arteries in the tissue sections of the control patient (between 5 and 17 Arteries were analyzed in three consecutive tissue sections of each patient). The measurement areas were identified by examining adjacent tissue sections, which were haematoxylin- and erythrosine-stained.

The raw spectra for each individual pixel were then imported into Matlab for further data processing and analysis. Each spectrum represents one pixel in one of the images recorded. Corrupted spectra containing NaNs were set to null vectors. The negative polarity mass spectra had a *m/z* range from 480 to 1900 with 0.005 amu intervals, which meant every spectrum or pixel consisted of a 190293-element vector. The total number of pixels equalled 191050 so the complete raw data set consisted of a 191050 × 190293 matrix. It was necessary to reduce the size of the raw data by reducing the spectra to 19029 element vectors (0.050 amu intervals) via interpolation (Figure S2). This 191050 × 19029 matrix was only about 29 Gb in size and therefore more manageable. All MALDI images were calibrated externally using a mixture of known peptides prior to their measurement, but because the images were recorded in different locations and on different tissue sections and on different days, slight *m/z* offsets were present from one image to another (Figure S3). This would negatively affect the data analysis, so all spectra were aligned using the mass peak at *m/z* 687.6 as a reference. The 2437 spectra, where this reference peak was absent, were set to null vectors. As a final step, the spectra were normalised using the total number of counts per pixel (Figure S4).

Because it is already known which samples are from PAH patient and which ones are from control patient, we decided to use a random forest (RF) classifier to analyse our data. Whereas PCA is an unsupervised data reduction method merely identifying linear correlation, RF is a supervised, tree-based learning algorithm, which works very well for classification problems[33]. It creates an ensemble of decision trees, using a randomly selected subset of training samples and variables, in order to predict class membership. This RF classifier can also rank the variables according to their ability to discriminate between the target classes, which is a great advantage given that the high dimensionality of our mass spectral data.

The training set was comprised of 5,000 randomly selected pixels from healthy data and 5,000 randomly selected pixels from PAH data, i.e. about 5% of the data set. 30 trees were produced to classify the pixels into two classes, namely healthy and PAH tissue, using Matlab's TreeBagger algorithm. An ensemble of 30 trees was deemed enough for this classification as the out-of-bag (OOB) error, an internal cross-validation metric for estimating the model's prediction error, stabilised around 12% and only marginally improved when the number of trees was increased (Figure S5).

This ensemble of bagged decision trees was then used to classify all pixels in the MALDI-ToF image data set. It was possible to distinguish PAH from control as nearly all pixels in our

MALDI images from control tissues were labelled "control tissue" and most of the pixels from the PAH tissues were labelled as "PAH tissue" (see Figure 1). This result clearly shows the RF classifier is capable of distinguishing PAH arteries from control arteries.

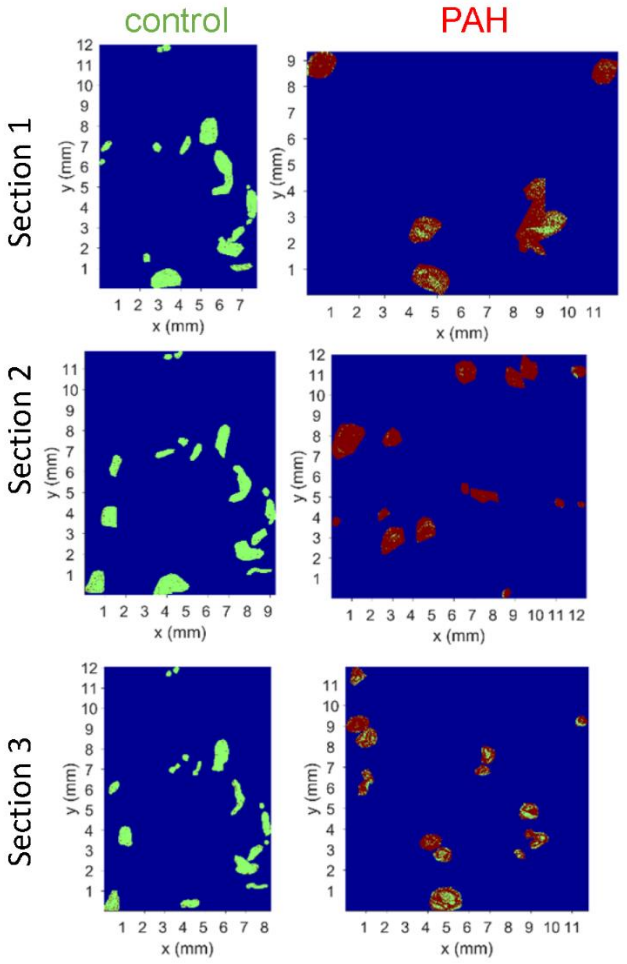

Figure 1. The random forest classification using 30 trees into control (green) and PAH (red) tissue from MALDI-TOF IMS data of three consecutive tissue sections from a control patient and three consecutive tissue sections from a PAH patient. It is clear the RF classifier is capable of distinguishing PAH tissue from control tissue based on their mass spectra.

By permuting out-of-bag observations among the trees we can furthermore estimate predictor importance values (Figure S6). Greater importance estimates indicate more important predictors. The top predictors (importance value > 0.4) correspond to maxima of mass peaks in our MALDI-ToF total mass spectrum, which indicates these mass peaks are potential markers for PAH. In order to verify if any of these 16 mass peaks can be used as markers for PAH, the average normalised ion intensities for all 16 peaks were calculated for each tissue section (Figure S7) and a two tailed t-test was used to determine if there were significant differences between PAH (n = 3 sections) and control tissue (n = 3 sections). Only the average normalised ion intensities for *m/z* 885.6, *m/z* 886.6 and *m/z* 887.7 were significantly different with P values of 0.01, 0.02 and 0.04, respectively. Based on their *m/z* values and relative intensities, these mass peaks could correspond with $[PI(38:4)-H]^-$ (1-octadecanoyl-2-(5Z,8Z,11Z,14Z-eicosatetraenoyl)-sn-glycero-3-phospho-(1'-myo-inositol), $C_{47}H_{82}O_{13}P^-$) and two peaks at M+1 and M+2 of the isotopic distribution. Using theoretical *m/z* values of 885.549853, 886.553208 and 887.556562, the measured *m/z* values deviated 68, 87 and 184 ppm, respectively. Ion images for the *m/z* 885.6 ion are shown in Figure 2.

The use of a RF classifier has helped us select the most relevant mass peaks, but this MALDI-ToF data originates from only one control and one PAH patient. In order to prove biological and clinical relevance of these potential marker ions, it is necessary to confirm the increased ion intensity for *m/z* 885.6 (and isotopic distributions at *m/z* 886.6 and 887.7) in multiple control and PAH patients. MALDI-TOF IMS measurements, however, are time-consuming due to the deposition of the matrix during the sample preparation and the slow image acquisition. We therefore decided to continue using another IMS technique, namely ToF-SIMS imaging. Both the sample preparation and data acquisition are a lot faster in the case of ToF-SIMS imaging and the use of a different IMS technique would be another way to validate our MALDI-ToF results.

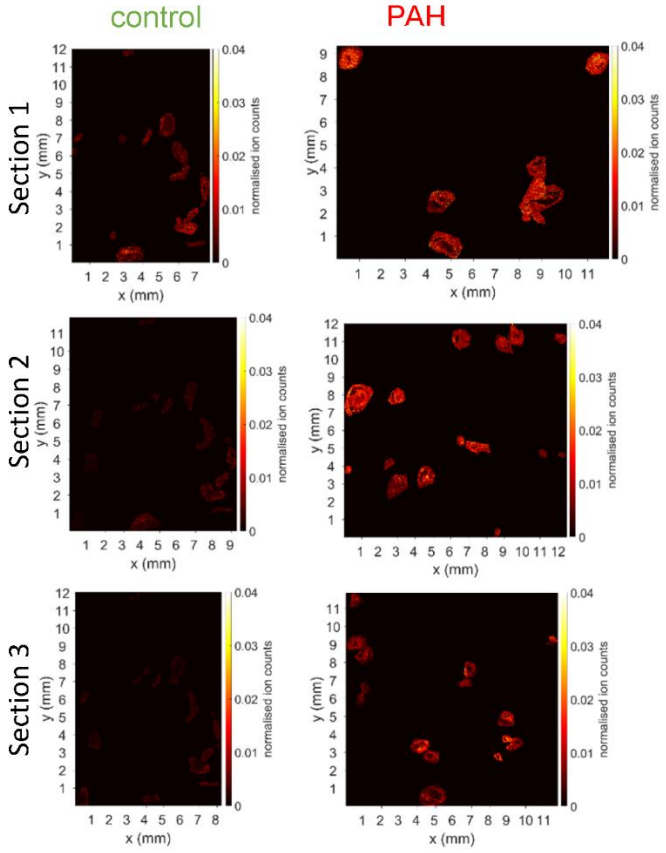

Figure 2. Negative polarity MALDI-TOF ion images of the mass peak at *m/z* 885.6 for three consecutive tissue sections from a control patient and three consecutive tissue sections from a PAH patient. The intensity of the *m/z* 885.6 $[PI(38:4)-H]^-$ ion is clearly higher in the tissue sections of the PAH patient compared to those of the control patient.

ToF-SIMS imaging. In order to demonstrate the increased intensity of the ion at *m/z* 885.6 in PAH tissue is indeed biologically relevant, ToF-SIMS images were acquired from three consecutive tissue sections of 5 PAH patients (IDs: PAH2, PAH3, PAH4, PAH5 and PAH6) and 4 control patients (IDs: CTRL2, CTRL3, CTRL4 and CTRL5). 5 arteries were measured on each dehydrated tissue section, which means a total of 75 arteries were imaged from PAH tissue and 60 arteries were

imaged from control tissue. Arteries were first identified using haematoxylin and erythrosine stained adjacent tissue sections.

The palmitate anion ($C_{16}H_{31}O_2^-$) at *m/z* 255.2 was chosen as a marker for biological tissue material in order to separate it from the OCT background (Figure S8). Via thresholding we then reconstructed mass spectra that excluded contributions from the OCT background. These reconstructed mass spectra were then imported into Matlab and interpolated to reduce the number of data points (Figure S9). Because the background for low intensity ions could be quite significant, a baseline correction was applied to the individual spectra (Figure S10). The spectra were then normalised to the total ion counts of the images to account for the differences in artery size as well as differences in the total ion intensity caused by topography and instrumental factors. In order to select all peaks in the mass spectra, all normalised mass spectra were summed, subjected to another baseline correction and then a peak search was performed identifying peaks with a minimum prominence of 0.008 and a maximum width of 0.325 amu (Figure S11). These values allowed all major peaks in the spectra to be selected and were determined empirically for these specific data sets. 1151 different mass peaks were selected, and their peak areas were calculated for all 135 spectra.

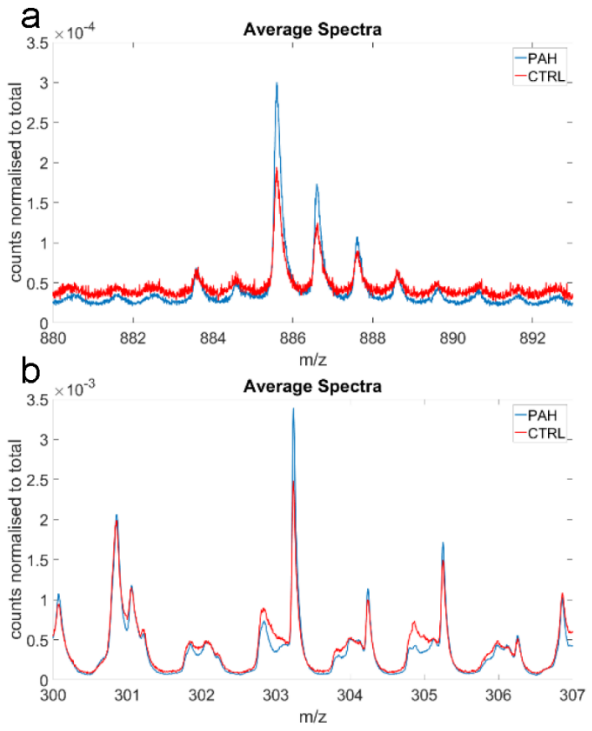

Figure 3. Details of the average, normalised negative polarity ToF-SIMS mass spectra for arterial tissue from PAH (n = 75) and control (n = 60) patients. A) The intensity of the $[PI(38:4)-H]^-$ monoisotopic ion at *m/z* 885.6 and its isotopes at *m/z* 886.6 and 887.7 are significantly higher (P = 0.0002, 0.0010 and 0.049, respectively) in the average mass spectrum for PAH arterial tissue. B). The intensity of the *m/z* 303.2 arachidonate anion is significantly higher (P = 0.0001) in the average mass spectrum for PAH arterial tissue.

One-way ANOVA on the *m/z* 885.6 signal of the 135 ToF-SIMS mass spectra of arterial tissue (75 PAH and 60 controls) showed there is a very highly significant difference detected when using the diagnosis as a factor (P = 0.0002). The average normalised ion intensity for the ion at *m/z* 885.6 is (4.4 ± 2.2) × 10^{-5} (n = 75) for arterial tissue from PAH patients and (3.0 ± 2.0) × 10^{-5} (n = 60) for arterial tissue from control patients (see Figure 3A). Logically, there is also a very highly significant difference between the nine patients (P < 0.0003). Within the PAH subset, there is no significant difference between the five individual patients (P = 0.1696), which indicates the signal at *m/z* 885.6 is equally elevated. Within the CTRL subset, there is a significant difference between the four individual patients (P < 0.0175), which indicates a degree of biological variation.

We have now shown that the increased intensity of the ion at *m/z* 885.6 in arterial tissue of PAH patients is indeed biologically relevant using a second IMS technique. Because we have peak areas for 1151 different mass peaks, we calculated their correlation coefficients in order to figure out which ions are positively correlated with our marker ion for PAH. When we limit our search to ions with a significant (P<0.05) correlation with the ion at *m/z* 885.6 and a correlation coefficient which is higher than 0.85, we not only find the presumed M+1 and M+2 isotopes at *m/z* 886.6 and 887.6 but also an ion at *m/z* 303.2 (see Figures 3A and 3B). One-way ANOVA further shows that the intensities of all three ions are significantly different between arterial tissue of PAH and that of control patients with P-values of 0.0010, 0.049 and 0.0001 respectively. The ion at *m/z* 303.2 could be attributed to the arachidonate anion ($C_{20}H_{31}O_2^-$), which means that, if the ion at *m/z* 885.6 is indeed phosphatidylinositol 38:4, its fatty acid configuration is likely composed of arachidonic and stearic acid. However, the only way to unambiguously identify the ion at *m/z* 885.6 is through tandem MS. We detected no significant difference (P > 0.05) in ion intensity at *m/z* 283.3 (stearate anion) when comparing control and PAH arterial tissue. However, considering that stearic acid is one of the most abundant fatty acids in mammalian tissue, it is likely that there are many lipid precursor ions that generate this fragment ion at *m/z* 283.3 and that the PI38:4 molecule only contributes little to the overall intensity of the ion at *m/z* 283.3.

MALDI MS/MS. Three areas of section 5 of PAH2 were analysed by MALDI MS/MS operating the TOF/TOF mass spectrometer in the so-called LIFT mode. The MS/MS fragment ion spectrum of the *m/z* 885.6 precursor ion (Figure S12) contains many ions characteristics of a PI(C18:0/C20:4) species. We can detect the $C_6H_{10}O_8P^-$ ion at *m/z* 241.0, which is a characteristic fragment for the inositol phosphate headgroup found in phosphatidylinositols (PIs)[34]. The fragment ions detected at *m/z* 283.3 and 303.2 correspond to the carboxylate anions of stearic ($C_{18}H_{35}O_2^-$) and arachidonic ($C_{20}H_{31}O_2^-$) acids, respectively. The signal at *m/z* 599.3 corresponds to the loss of arachidonic acid as ketene from the precursor ion at *m/z* 885.6, the ion at *m/z* 581.3 corresponds to the neutral loss of arachidonic acid from the precursor ion at *m/z* 885.6 and the signal at *m/z* 419.3 corresponds to the neutral loss of arachidonic acid and inositol from the precursor ion at *m/z* 885.6. This clearly confirms arachidonic acid as a part of the fatty acid composition. Finally, the peak at *m/z* 153.0 corresponds to a glycerol-3-phosphate ion with loss of H_2O ($C_3H_6O_5P^-$). A possible chemical structure of PI(C18:0/C20:4) is shown in Figure S13 and agrees with already published MS/MS analysis of this ion species[31] as well as commonly occurring product ions published online in LIPIDMAPS[35]. Although neither the relative sn-1 or sn-2 position of the fatty acids, nor the position of the double bonds in the C20:4 can be determined by the MS/MS analysis, this confirms that the ion at *m/z* 885.6 in our previous MALDI analyses is PI(C18:0/C20:4).

Hybrid SIMS MS/MS. In order to unambiguously identify the ion at *m/z* 885.6 observed in our ToF-SIMS analyses, one area of section 5 of PAH6 was analysed using IONTOF's new Hybrid SIMS Instrument. The MS/MS fragment ion spectrum of the *m/z* 885.551 precursor ion (see Figure 4) is very similar to the ones obtained using MALDI MS/MS. We are able to detect the $C_6H_8O_7P^-$ ion at *m/z* 223.001 and the $C_6H_{10}O_8P^-$ ion at *m/z* 241.012, which are characteristic fragments for the inositol phosphate headgroup found in phosphatidylinositols (PIs). The fragment ions at *m/z* 283.264 and 303.233 correspond to the carboxylate anions of stearic ($C_{18}H_{35}O_2^-$) and arachidonic ($C_{20}H_{31}O_2^-$) acid. The signal at *m/z* 581.310 corresponds to the neutral loss of arachidonic acid from the precursor ion at *m/z* 885.551 and the signal at *m/z* 419.257 corresponds to the neutral loss of arachidonic acid and inositol from the precursor ion at *m/z* 885.551. Finally, the peaks at *m/z* 78.959 and 152.996 correspond to the PO_3^- ion and a glycerol-3-phosphate ion with loss of H_2O ($C_3H_6O_5P^-$), respectively. Thanks to the ultrahigh mass resolution of the Orbitrap equalling 211,781 at *m/z* 303.233, it was possible to assign chemical formulas to the peaks with a mass accuracy smaller than 1 ppm. This confirms that the ion at *m/z* 885.6 in the previous ToF-SIMS imaging analyses is PI(C18:0/C20:4).

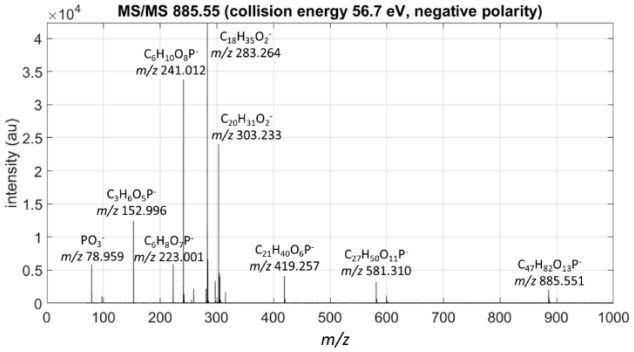

Figure 4. The negative polarity MS/MS fragment ion spectrum (collision energy of 56.7 eV) of the *m/z* 885.551 precursor ion from PAH arterial tissue recorded using the Hybrid SIMS Orbitrap Instrument. The MS/MS fragment ion spectrum contains many ions characteristic of a PI C18:0/C20:4 species such as the $C_6H_8O_7P^-$ ion at *m/z* 223.001 and the $C_6H_{10}O_8P^-$ ion at *m/z* 241.012, which are characteristic fragments for the inositol phosphate headgroup, and the $C_{18}H_{35}O_2^-$ ion at *m/z* 283.264 and the $C_{20}H_{31}O_2^-$ ion at *m/z* 303.233 corresponding to stearic and arachidonic acid, respectively.

Discussion

In this study, we showed that remodeled pulmonary arteries of PAH patients present higher levels of PI(C18:0/C20:4) than healthy pulmonary arteries from control subjects. To our knowledge this is a new insight in the field of PAH research, which has been made possible thanks to the combined use of TOF-SIMS and MALDI IMS for marker discovery, and MS/MS for validation of the ion identity.

Cellular lipids have numerous roles within a cell. Although PIs have no known signalling activity, they are critical messenger precursors and part of the so-called PI cycle (Figure S14). The PI cycle takes place between the endoplasmic reticulum (ER) and the plasma membranes. In the ER membrane, phosphatidic acid (PA) derives from glycerol 3-phosphate (G3P) by two successive acylation reactions. Once synthesized, PA is used as a precursor for the synthesis of cytidine diphosphate diacylglycerol (CDP-DG) by the CDP-DG synthases (CDS1/2)[36,37]. Finally, the PI synthase (PIS) links a CDP-DG to an inositol which forms the terminal PI. This PI is then transported from the ER membrane to the plasma membrane by the phosphatidylinositol transfer protein (PITP), where it is sequentially phosphorylated by phosphoatidylinositol 4-kinase (PI4K) and PI5K to give PI 4,5-bisphosphate (PIP2). Upon stimulus-induced phospholipase C (PLC) activation, PIP2 is cleaved into two lipids: inositol 1,4,5-trisphosphate (IP3) and diacylglycerol (DAG), which are important second messengers[37]. Among the multiple roles of DAG, it can be phosphorylated by the diacylglycerol kinase (DGK) family, which gives a new PA and restarts the PI cycle (Figure S14).

Furthermore, PI3K phosphorylates PIP_2 to form IP3, whereas PTEN dephosphorylates IP3 to PIP_2. Although no study showed differences in expression or activation levels of PI3K and PTEN in PAH until now, it is known that Cowden syndrome-associated PAH is caused by germline mutations of PTEN. In addition, differences in expression or activation levels of PI3K and PTEN have been demonstrated for pulmonary vascular remodelling in animal models. In hypoxia- and MCT-induced PH in the rat, PTEN lung protein expression is decreased[38]. On the other hand, PI3K is more activated in MCT-treated rats compared with control littermates[39,40]. In cancers and particularly in lung cancers, increased activity of PI3K as well as decreased activity of PTEN are known to participate in aberrant cell proliferation[41]. Therefore, there is some indication IP3 could be involved in PAH.

IP3 can activate its receptor (IP3R) on the ER membrane, which induces Ca_2^+ release from ER stocks and subsequent rise in cytosolic [Ca_2^+]. Increases in the concentration of Ca_2^+ and DAG are known to activate protein kinase C (PKC) enzymes, which in turn activate other cytosolic proteins by phosphorylation. We hypothesize that PI(38:4) as a precursor for PIP_2 might be a major source of IP3 and DAG, which triggers a powerful proliferative signal for the cells.

If this hypothesis is correct, because it is secreted by the pulmonary vascular cells, PI(C18:0/C20:4) may be a useful PAH diagnostic biomarker if one could dose it in blood. Dosage in the circulation would be preferred in this case because lung biopsy is risky and not in practice in PAH patient management. It could also become a possible therapeutic target by blocking enzymes responsible for its biosynthesis, if such inhibitors could specifically target the pulmonary circulation or even the over-proliferative pulmonary vascular cells to overcome adverse effects.

However, we are aware of the limitations of the present study: further work is needed to confirm these results on a larger cohort of PAH patients. Since the patients studied had end-stage PAH, it would be interesting to assess the stage of the disease in which PI levels start to significantly differ with controls in a diagnostic perspective by following PI levels in the circulation. Finally, animal models of experimental PH should be used to re-express PTEN in the pulmonary circulation, or to study in-depth the mechanism of DGK or CDS1/2 inhibition.

Conclusions

We were able to chemically image human lung tissue from PAH patients and compare the results with lung tissue from control patients. In a first step, we compared MALDI-ToF im-

age data from tissue sections of one PAH and one control patient. Due to the complexity of the IMS data, it was necessary to use advanced data analysis tools. In this work, we demonstrate the potential of a random forest (RF) classifier on mass spectrometric image data. The RF classifier successfully identifies individual pixels in the MALDI-ToF IMS data as PAH or control tissue and makes the selection of the most relevant mass peaks less time-consuming, less error-prone and less subjective. In our study, using the RF classifier, the monoisotopic ion at *m/z* 885.6 was identified as a relevant marker for PAH. Using a second IMS technique, ToF-SIMS imaging, we were able to analyze 75 arteries from 5 PAH patients and 60 arteries from 4 control patients and proved that the same ion at *m/z* 885.6 is indeed a biologically relevant marker for PAH. Tandem mass spectrometry measurements performed using a MALDI-ToF/ToF and a SIMS, which is capable of MS/MS with high mass resolution, were then used to unambiguously identify the ion at *m/z* 885.6 as a PI C18:0/C20:4 species. This study is the first to highlight increased levels of PI(38:4) in the remodelled pulmonary arteries of PAH patients. Having identified this molecule a potential biomarker of PAH, we can now use this knowledge to gain further insight into its role in the disease mechanism. More importantly, this work demonstrates the potential of IMS for biomarker discovery, which in turn could lead to novel approaches for early diagnosis and targeted drug development.

ASSOCIATED CONTENT

Supporting Information

The Supporting Information is available free of charge on the ACS Publications website.
Table S1 and Figures S1-S14 (PDF)

AUTHOR INFORMATION

Corresponding Authors

*E-mail: alain.brunelle@cnrs.fr.
*E-mail: sylvia.cohen-kaminsky@universite-paris-saclay.fr.

ORCID

Sebastiaan Van Nuffel: 0000-0003-1251-3236
Marceau Quatredeniers: 0000-0002-7862-1320
Jean-Pierre Le Caer: 0000-0002-9668-4747
Nicolas Elie: 0000-0002-8733-0971
Quentin Vanbellingen: 0000-0003-3894-638X
Sébastien Joël Dumas: 0000-0001-9958-3485
Morad Kamel Nakhleh: 0000-0001-7472-750X
Maria-Rosa Ghigna: 0000-0001-5996-665X
Elie Fadel: 0000-0002-9290-4589
Marc Humbert: 0000-0003-0703-2892
Pierre Chaurand: 0000-0001-6821-7001
David Touboul: 0000-0003-2751-774X
Sylvia Cohen-Kaminsky: 0000-0002-6341-7482
Alain Brunelle: 0000-0001-6526-6481

Present Addresses

† Materials Research Institute, The Pennsylvania State University, University Park, Pennsylvania 16802, USA.
‡ Center of Expertise in Drug Safety & Pharmacokinetics, Technologie Servier, 25/27 rue Eugène Vignat – CS 11749 – F-45007 Orléans, Cedex 1, France
§ Laboratory of Angiogenesis and Vascular Metabolism, Department of Oncology, KU Leuven, Center of Cancer Biology, VIB, Leuven, B-3000, Belgium

Author Contributions

S.V.N. designed the study, performed experiments and data analysis, and wrote the main manuscript. M.Q. assisted with experimental design, prepared samples for IMS and wrote the main manuscript. A.P. and J.Z. performed all Hybrid SIMS experiments. J.P.L.C. performed all MALDI-TOF IMS measurements. N.E. performed ToF-SIMS imaging experiments and MALDI MS/MS measurements. Q.V.B performed exploratory ToF-SIMS imaging experiments and analysis. S.J.D. prepared exploratory samples for IMS. M.K.N. assisted with data analysis. M.R.G. performed all pathology assessments. E.F. was responsible for human tissue banking. M.H. and D.T. assisted with experimental design and writing of the manuscript. P.C., S.C.K. and A.B. designed the study and wrote the main manuscript. / †† These authors contributed equally.

ACKNOWLEDGMENT

This work was financially supported by the Agence Nationale de la Recherche (France, grant ANR-2015-CE29-0007-01 and-02 DEFIMAGE) and by the Idex Paris-Saclay Jean d'Alembert fellowship program (France). The work was supported by LabEx LERMIT, Laboratory of Excellence in Research on Medication and Innovative Therapeutics under the Investment for the Future program Agence Nationale de la Recherche (ANR)-11-IDEX-0003-01 within the ANR-10-LABX-0033 (to S.C.K.), Département Hospitalo-Universitaire Thorax Innovation, and Assistance Publique-Hôpitaux de Paris. This work was also funded by Institut National de la Santé Et de la Recherche Médicale (INSERM), Université Paris-Sud, and Hôpital Marie Lannelongue. The authors would also like to thank the French Pulmonary Hypertension Registry facilities and the French National Referral Center for Severe Pulmonary Hypertension for providing clinical samples and data. In particular, the authors thank Pr. Olaf Mercier, Pr. Dominique Fabre and Dr. Sasha Mussot, surgeons in the *Service de Chirurgie Thoracique & Vasculaire* from *Hôpital Marie Lannelongue* for providing quality human lung tissue samples, as well as Caroline Communaux in the *Service d'Anatomopathologie* for providing clinical data. The authors would also like to thank Dr. Alex Henderson for the insightful discussions regarding supervised machine learning.

REFERENCES

[1] Galiè, N.; Humbert, M.; Vachiery, J.L.; Gibbs, S.; Lang, I.; Torbicki, A.; Simonneau, G.; Peacock, A.; Vonk Noordegraaf, A.; Beghetti, M.; Ghofrani, A. ESC/ERS Guidelines for the diagnosis and treatment of pulmonary hypertension: The Joint Task Force for the Diagnosis and Treatment of Pulmonary Hypertension of the European Society of Cardiology (ESC) and the European Respiratory Society (ERS): Endorsed by: Association for European Paediatric and Congenital Cardiology (AEPC), International Society for Heart and Lung Transplantation (ISHLT). *Eur. Respir. J.*, **2015**, 46, 903–975.

[2] Galiè, N.; McLaughlin, V.V.; Rubin, L.J.; Simonneau, G. An overview of the 6th World Symposium on Pulmonary Hypertension. *Eur. Respir. J.* **2019**, 53, 1802148.

[3] Chughtai, K.; Heeren, R.M.A. Mass spectrometric imaging for biomedical tissue analysis. *Chem. Rev.* **2010**, 110, 3237-3277.

[4] Bich, C.; Touboul, D.; Brunelle, A. Biomedical studies by TOF-SIMS imaging. *Biointerphases* **2015**, 10, 018901.

[5] Gilmore, I.S.; Heiles, S.; Pieterse, C.L. Metabolic imaging at the single-cell scale: recent advances in mass spectrometry imaging. *Annu. Rev. Anal. Chem.*, **2019**, 12, 201-224.
[6] Bodenmiller, B. Multiplexed Epitope-Based Tissue Imaging for Discovery and Healthcare Applications. *Cell Systems*, **2016**, 2, 225-238.
[7] Passarelli, Melissa K.; Winograd, N. Lipid imaging with time-of-flight secondary ion mass spectrometry (ToF-SIMS). *BBA-Mol. Cell. Biol. L.*, **2011**, 1811, 976-990.
[8] Bich, C.; Touboul, D.; Brunelle, A. Cluster TOF-SIMS imaging as a tool for micrometric histology of lipids in tissue. *Mass Spectrom. Rev.*, **2014**, 33, 442-451.
[9] Schaepe, K.; Bhandari, D.R.; Werner, J.; Henss, A.; Pirkl, A.; Kleine-Boymann, M.; Rohnke, M.; Wenisch, S.; Neumann, E.; Janek, J.; Spengler, B. Imaging of Lipids in Native Human Bone Sections Using TOF–Secondary Ion Mass Spectrometry, Atmospheric Pressure Scanning Microprobe Matrix-Assisted Laser Desorption/Ionization Orbitrap Mass Spectrometry, and Orbitrap–Secondary Ion Mass Spectrometry. *Anal. Chem.* **2018**, 90, 8856-8864.
[10] Lothar, V.; Vennemann, A.; Breitenstein, D.; Engelhard, C.; Wiemann, M.; Hagenhoff, B. Detection of SiO2 nanoparticles in lung tissue by ToF-SIMS imaging and fluorescence microscopy. *Analyst*, **2017**, 142, 2631-2639.
[11] Lothar, V.; Böttner, J.; Vennemann, A.; Breitenstein, D.; Engelhard, C.; Meijer, J.; Estrela-Lopis, I.; Wiemann, M.; Hagenhoff, B. Detection of ZrO2 Nanoparticles in Lung Tissue Sections by Time-of-Flight Secondary Ion Mass Spectrometry and Ion Beam Microscopy. *Nanomaterials*, **2018**, 8, 44.
[12] Lothar, V.; Vennemann, A.; Breitenstein, D.; Engelhard, C.; Hagenhoff, B.; Wiemann, M. Distribution of Paramagnetic Fe2O3/SiO2–Core/Shell Nanoparticles in the Rat Lung Studied by Time-of-Flight Secondary Ion Mass Spectrometry: No Indication for Rapid Lipid Adsorption. *Nanomaterials*, **2018**, 8, 571.
[13] Lothar, V.; Dietrich, D.; Vennemann, A.; Breitenstein, D.; Engelhard, C.; Karst, U.; Sperling, M.; Wiemann, M.; Hagenhoff, B. Combination of micro X-ray fluorescence spectroscopy and time-of-flight secondary ion mass spectrometry imaging for the marker-free detection of CeO 2 nanoparticles in tissue sections. *J. Anal. Atom. Spectrom.*, **2018**, 33, 491-501.
[14] Carado, A.; Kozole, J.; Passarelli, M.; Winograd, N.; Loboda, A.; Bunch, J.; Wingate, J.; Hankin, J.; Murphy, R. Biological tissue imaging with a hybrid cluster SIMS quadrupole time-of-flight mass spectrometer. *Appl. Surf. Sci.*, **2008**, 255, 1572-1575.
[15] Desbenoit, N.; Saussereau, E.; Bich, C.; Bourderioux, M.; Fritsch, J.; Edelman, A.; Brunelle, A.; Ollero, M. Localized lipidomics in cystic fibrosis: TOF-SIMS imaging of lungs from Pseudomonas aeruginosa-infected mice. *Int. J. Biochem. Cell B.*, **2014**, 52, 77-82.
[16] Najafinobar, N.; Venkatesan, S.; von Sydow, L.; Klarqvist, M.; Olsson, H.; Zhou, X.H.; Cloonan, S.M.; Malmberg, P. ToF-SIMS mediated analysis of human lung tissue reveals increased iron deposition in COPD 5GOLD IV) patients. *Sci. Rep.*, **2019**, 9, 10060, 1-9.
[17] Dumas, S.J.; Bru-Mercier, G.; Courbourlin, A.; Quatredeniers, M.; Rücker-Martin, C.; Antigny, F.; Nakhleh, M.K.; Ranchoux, B.; Gouadon, E.; Vinhas, M.C.; Vocelle, M.; Raymond, N.; Dormüller, P.; Fadal, E.; Perros, F.; Humbert, M.; Cohen-Kaminsky, S. NMDA-Type glutamate receptor activation promotes vascular remodelling and pulmonary arterial hypertension. *Circulation*, **2018**, 137, 2371-2389.
[18] Gilmore, I.S., SIMS of organics—Advances in 2D and 3D imaging and future outlook. *J. Vac. Sci. Technol. A*, **2013**, 31, 050819.
[19] Fletcher, J.S.; Vickerman, J.C.; Winograd, N. Label free biochemical 2D and 3D imaging using secondary ion mass spectrometry. *Curr. Opin. Chem. Biol.*, **2011**, 15, 733-740.
[20] Graham, D.J.; Castner, D.G. Multivariate analysis of ToF-SIMS data from multicomponent systems: the why, when, and how. *Biointerphases*, **2012**, 7, 49.
[21] Tyler, B.J.; Rayal, G.; Castner, D.G. Multivariate analysis strategies for processing ToF-SIMS images of biomaterials. *Biomaterials*, **2007**, 28, 2412-2423.
[22] Trindade, G.F.; Abel, M.L.; Watts, J.F. simsMVA: A tool for multivariate analysis of ToF-SIMS datasets. *Chemometr. Intell. Lab.*, **2018**, 182, 180-187.
[23] Van Nuffel, S.; Parmenter, C.; Scurr, D.J.; Russell, N.A.; Zelzer, M. Multivariate analysis of 3D ToF-SIMS images: method validation and application to cultured neuronal networks. *Analyst*, **2016**, 141(1), 90-95.
[24] Van Nuffel, S.; Elie, N.; Yang, E.; Nouet, J.; Touboul, D.; Chaurand, P.; Brunelle, A. Insights into the MALDI process after matrix deposition by sublimation using 3D ToF-SIMS imaging. *Anal. Chem.*, **2018**, 90, 1907-1914.
[25] Hanselmann, M.; Köthe, U.; Kirchner, M.; Renard, B.Y.; Amstalden, E.R.; Glunde, K.; Heeren, R.M.A.; Hamprecht, F.A. Toward digital staining using imaging mass spectrometry and random forests. *J. Proteome Res.*, **2009**, 8, 3558-3567.
[26] Tian, X.; Zhang, G.; Shao, Y.; Yang, Z. Towards enhanced metabolomic data analysis of mass spectrometry image: Multivariate Curve Resolution and Machine Learning. *Anal. Chim. Acta*, **2018**, 1037, 211-219.
[27] Angerer, T.B.; Velickovic, D.; Nicora, C.D.; Kyle, J.E.; Graham, D.J.; Anderton, C.R.; Gamble, L.J. Exploiting the semi-destructive nature of GCIB-ToF-SIMS imaging for simultaneous localization and confident lipid annotations. *Anal. Chem.*, **2019**, 91, 15073−15080.
[28] Passarelli, M.K.; Pirkl, A.; Moellers, R.; Grinfeld, D.; Kollmer, F.; Havelund, R.; Marshall, P.S.; Arlinghaus, H.; Alexander, M.R.; West, A.; Horning, S.; Niehuis, E.; Makarov, A.; Dollery, C.T.; Gilmore, I. S. The 3D OrbiSIMS—label-free metabolic imaging with subcellular lateral resolution and high mass-resolving power. *Nat. Methods*, **2017**, 14, 1175-1183.
[29] Eliuk, S.; Makarov, A. Evolution of orbitrap mass spectrometry instrumentation. *Annu. Rev. Anal. Chem.*, **2015**, 8, 61-80.
[30] Thomas, A.; Charbonneau, J.L.; Fournaise, E.; Chaurand, P. *Anal. Chem.* **2012**, 84, 2048-2054.
[31] Cerruti, C.D.; Benabdellah, F.; Laprévote, O.; Touboul, D.; Brunelle, A. MALDI imaging and structural analysis of rat brain lipid negative ions with 9-aminoacridine matrix. *Anal. Chem.*, **2012**, 84, 2164-2171.
[32] Sodhi, R.N.S *Analyst* **2004**, 129, 483-487.
[33] Breiman, L. Random Forests. *Mach. Learn.*, **2001**, 45, pp. 5–32.
[34] Touboul, D.; Brunelle, A.; Halgand, F.; De La Porte, S.; Laprévote, O. Lipid imaging by gold cluster time-of-flight secondary ion mass spectrometry: application to Duchenne muscular dystrophy. *J. Lip. Res.*, **2005**, 46, 1388-1395.
[35] https://www.lipidmaps.org
[36] Cockcroft, S.; Raghu, P. Topological organisation of the phosphatidylinositol 4,5-bisphosphate-phospholipase C resynthesis cycle: PITPs bridge the ER-PM gap. *Biochem. J.*, **2016**, 473, 4289–4310.
[37] Epand, R. M. Features of the Phosphatidylinositol Cycle and its Role in Signal Transduction. *J. Membrane Biol.*, **2017**, 250, 353–366.
[38] Ravi, Y.; Selvendiran, K.; Meduru, S.; Citro, L.; Naidu, S.; Khan, M.; Rivera, B.K.; Sai-Sudhakar, C.B.; Kuppusamy, P. Dysregulation of PTEN in Cardiopulmonary Vascular Remodeling Induced by Pulmonary Hypertension. *Cell Biochem. Biophys.*, **2013**, 67, 363–372.
[39] Zha, L.H.; Zhou, J.; Li, T.Z.; Luo, H.; Zhang, M.Q.; Li, S.; Yu, Z.X. NLRC3 inhibits MCT-induced pulmonary hypertension in rats via attenuating PI3K activation. *J. Cell. Physiol.*, **2019**, 234, 15963-15976.
[40] Goncharova, E.A.; Ammit, A.J.; Irani, C.; Carroll, R.G.; Eszterhas, A.J.; Panettieri, R.A.; Krymskaya, V.P. PI3K is required for proliferation and migration of human pulmonary vascular smooth muscle cells. *Am. J. Physiol. Lung Cell. Mol. Physiol.*, **2002**, 283, L354-363.
[41] Pérez-Ramírez, C.; Cañadas-Garre, M.; Molina, M.Á.; Faus-Dáder, M.J.; Calleja-Hernández, M.Á. PTEN and PI3K/AKT in non-small-cell lung cancer. *Pharmacogenomics*, **2015**, 16, 1843–1862.

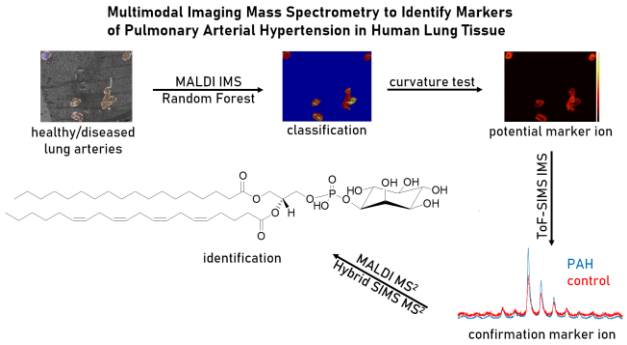
Multimodal Imaging Mass Spectrometry to Identify Markers
of Pulmonary Arterial Hypertension in Human Lung Tissue
MALDI IMS
Random Forest
curvature test
healthy/diseased
lung arteries
classification
potential marker ion
ToF-SIMS IMS
identification
MALDI MS²
Hybrid SIMS MS²
PAH
control
confirmation marker ion

Figure 1

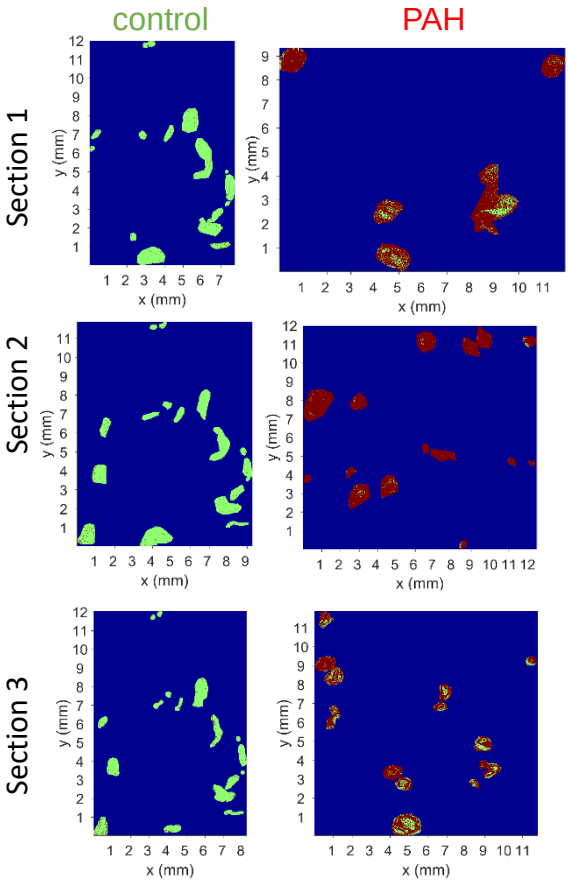

Figure 2

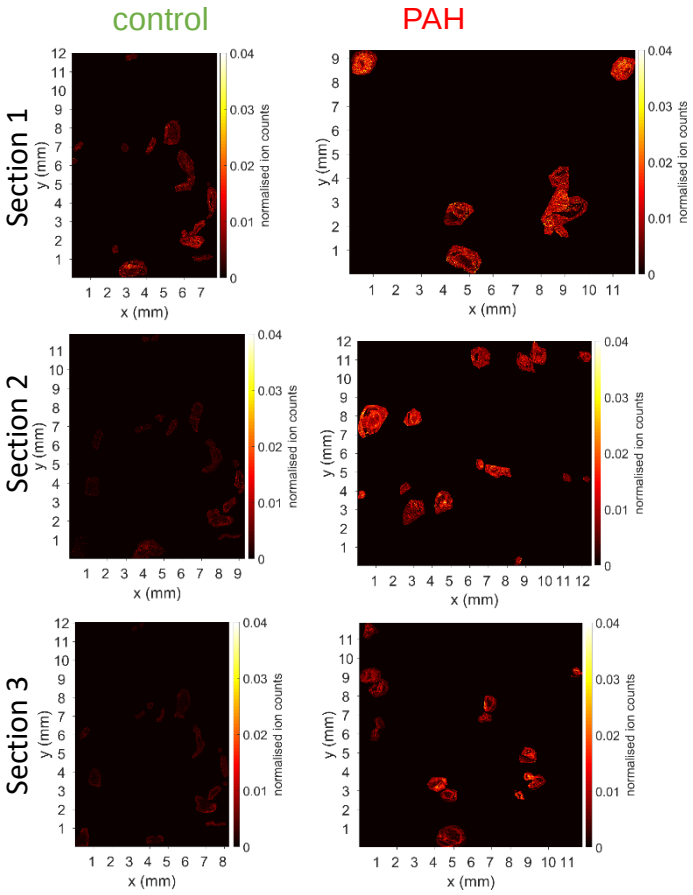
control
PAH
Section 1
Section 2
Section 3
y (mm)
x (mm)
normalised ion counts
0.04
0.03
0.02
0.01
0

Figure 3

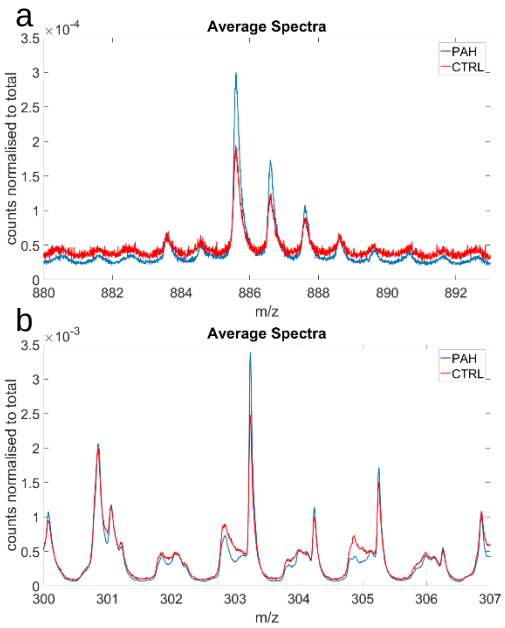
a
Average Spectra
×10^-4
3.5
3
2.5
2
1.5
1
0.5
0
counts normalised to total
PAH
CTRL
880
882
884
886
888
890
892
m/z
b
Average Spectra
×10^-3
3.5
3
2.5
2
1.5
1
0.5
0
counts normalised to total
PAH
CTRL
300
301
302
303
304
305
306
307
m/z

Figure 4

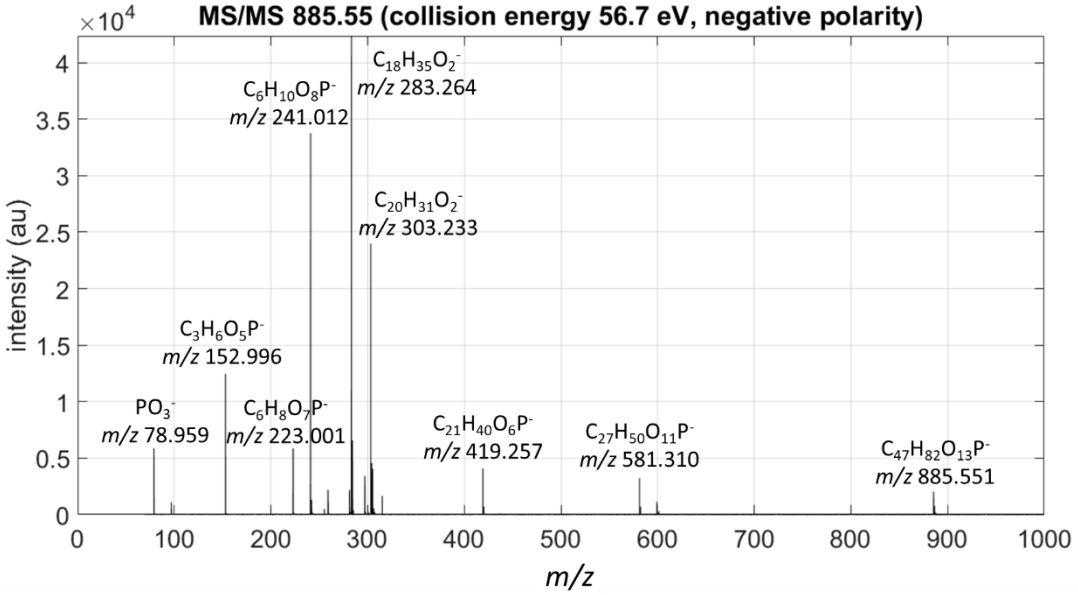
MS/MS 885.55 (collision energy 56.7 eV, negative polarity)
×10^4
intensity (au)
m/z
C18H35O2- m/z 283.264
C6H10O8P- m/z 241.012
C20H31O2- m/z 303.233
C3H6O5P- m/z 152.996
PO3- m/z 78.959
C6H8O7P- m/z 223.001
C21H40O6P- m/z 419.257
C27H50O11P- m/z 581.310
C47H82O13P- m/z 885.551

Multimodal Imaging Mass Spectrometry to Identify Markers of Pulmonary Arterial Hypertension in Human Lung Tissue

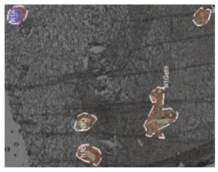

healthy/diseased lung arteries

MALDI IMS
Random Forest

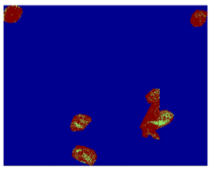

classification

curvature test

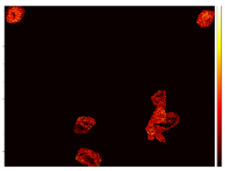

potential marker ion

ToF-SIMS IMS

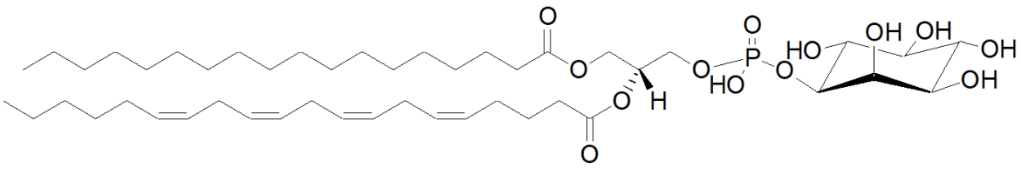

identification

MALDI MS^2
Hybrid SIMS MS^2

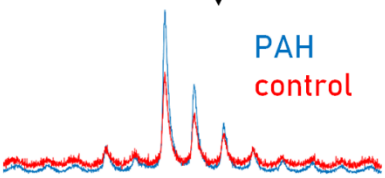

confirmation marker ion